Interference Modeling for Low-Height Air-to-Ground Channels in Live LTE Networks

Cai, Xuesong; Zhang, Chao; Rodríguez-Piñeiro, José ; Yin, Xuefeng; Fan, Wei; Pedersen, Gert Frølund

Published in:
IEEE Antennas and Wireless Propagation Letters

DOI (link to publication from Publisher):
10.1109/LAWP.2019.2936264

Publication date:
2019

Document Version
Accepted author manuscript, peer reviewed version

Interference Modeling for Low-Height Air-to-Ground Channels in Live LTE Networks

Xuesong Cai, Chao Zhang, José Rodríguez-Piñeiro, Xuefeng Yin, *Member, IEEE*, Wei Fan, and Gert Frølund Pedersen, *Senior Member, IEEE*

***Abstract*—In this letter, a recently conducted measurement campaign in two suburban scenarios for investigating the low-height air-to-ground channels is presented. A Universal Software Radio Peripheral (USRP)-based channel sounder on-board a unmanned-aerial-vehicle (UAV) was exploited to record the real-time down-link signals of the live Long Term Evolution (LTE) networks. Several horizontal flights at different heights were conducted in the measurement campaign. Channel impulse responses (CIRs) of links from the UAV to different live cells were extracted by exploiting the cell reference specific signals (CRSs) received in the down-link data. By using the empirical CIRs, a maximization-likelihood estimator is derived based on the Space-Alternating Generalized Expectation-Maximization (SAGE) principle to obtain the signal power for individual channels between multiple base stations and the UAV. Interference, detected cells number, handover rate etc. are studied, which provide insights to understand interference for low-height air-to-ground channels.**

***Index terms*—** Air-to-ground, propagation channel, UAV, interference and LTE.

I. Introduction

Unmanned aerial vehicles (UAVs) are now rapidly expanding their market to commercial, scientific, agriculture and recreational areas [1]–[5]. The air-to-ground (A2G) channel can give support to different types of communications [5], such as high-throughput data traffic from UAV to ground stations (e.g. real-time video surveillance) and control and non-payload communications (CNPC) where low-throughput data but highly requiring reliability and low-latency (e.g. flight commands) are transmitted from ground stations to UAVs.

It is widely expected that the commercial or live cellular deployments, e.g. the Long Term Evolution (LTE) networks originally aimed for terrestrial coverage, will give access to UAV connectivity, as the flight heights of UAVs have been limited under around 100 m or 150 m in many countries [6]. Study item [7] and work item [8] have been approved by the 3rd Generation Partnership Project (3GPP) to investigate the underlying feasibility of exploiting the existing LTE networks to enable an early stage of UAV-based applications. Since accurate channel model is a prerequisite for communication systems [5], [9], [10], understanding the A2G propagation channel between UAVs and LTE base stations is critical. Multiple research activities have studied the A2G channel characteristics between an UAV and a ground base station in live LTE cellular networks. The authors in [11] claim that the path loss is a composite effect of the empirical base-station configuration and the propagation channel, depending on the angle between the UAV and the base-station. In [12], authors suggest to use height-dependent path loss models based on field measurements at 800 MHz. The measurement results demonstrate that better radio clearance is achieved due to the visual line-of-sight (LoS) as the UAV moves up, which also indicates probably more interference from neighboring cells [13]. Interference is one of the main aspects that need to be considered for aerial users. Basically, neighboring base stations and up-link communications from the other UAVs are main factors leading to non-negligible interference for aerial users. In [14], authors proposed a new cooperative non-orthogonal multiple access (NOMA) technique to mitigate the uplink interference by jointly optimizing the UAV's rate and power allocations. In [15], different beamforming techniques have been evaluated for downlink interference cancelling for UAV communications.

Although investigations have been done in terms of interference cancellation for UAV communications, realistic modeling of interference in live LTE networks based on real field measurements is still inadequate. The unrealistic interference levels based on either assumption or simulation could bias the performance evaluation results. It is in necessity to understand the interference characteristics in realistic LTE networks considering the effects of real environment type, cell type and flight height. In this letter, a measurement campaign is presented where a USRP-based channel sounder on-board a UAV is exploited. The channel characteristics experienced by the sounder own high fidelity to the real aerial users in LTE networks. Two different suburban scenarios are considered, where the cell types are different. In each scenario, five horizontal flights at different heights were conducted. Based on the Space-Alternating Generalized Expectation-Maximization (SAGE) estimation results, interference characteristics are elaborated for the two scenarios.

The rest of this letter is organized as follows. Sec. II elaborates the measurement scenarios and channel sounder. Sect. III elaborates the data processing, interference investigation, and modeling for the two scenarios. Finally, conclusive remarks are included in Sect. IV.

X. Cai, C. Zhang, W. Fan and G. Frølund Pedersen are with the APMS section at the Department of Electronic Systems, Falculty of Engineering and Science, Aalborg University, Aalborg 9220, Denmark (e-mail: xuc@es.aau.dk; czhang@es.aau.dk; wfa@es.aau.dk, gfp@es.aau.dk).

J. Rodríguez-Piñeiro and X. Yin are with the College of Electronics and Information Engineering, Tongji University, Shanghai 201804, China (email: j.rpineiro@tongji.edu.cn; yinxuefeng@tongji.edu.cn).

(a) Scenario A (b) Scenario B

Fig. 1: Two suburban scenarios in the measurement campaign. The red dots indicate example locations of base stations in the illustrated area.

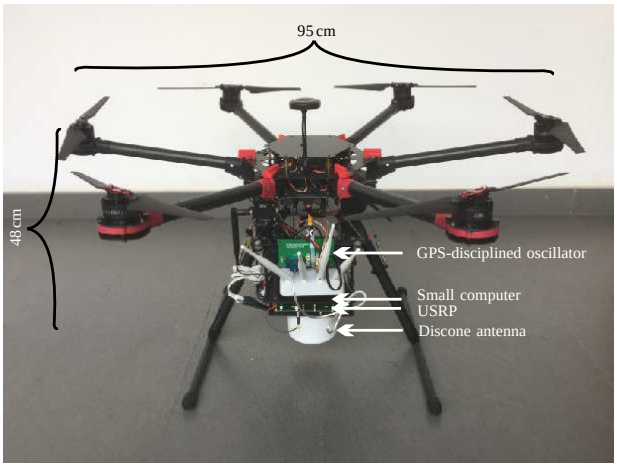

Fig. 2: The USRP-based channel sounder on-board the UAV used in the measurement campaign.

II. Measurement campaign

The measurement campaign was conducted in two suburban scenarios at the campus of Tongji University, Shanghai, China. Fig. 1(a) and Fig. 1(b) illustrate the satellite views of the two scenarios, i.e. scenario A and scenario B. Basically, the two scenarios are characterized by trees, buildings and rivers (or water). Scenario A is more open than scenario B as we can observe that the building density in scenario B is much higher than that in scenario A. Therefore, the base stations (BSs) in scenario A are observed typically with heights around 20 to 30 m and low density, while BSs in scenario B are typically with heights around 10 to 15 m and larger density. As indicated by the white lines in both figures, five horizontal flight-routes were performed respectively in the two scenarios. In scenario A, the five horizontal flights were conducted at the heights of 15, 35, 50, 75 and 100 m, and the horizontal distance for each flight was 500 m. In scenario B, the five horizontal flights were conducted at the heights of 35, 50, 65, 80 and 100 m, and the horizontal distance was 450 m for each flight.[1]

Fig. 2 illustrates the channel sounder on-board a UAV exploited in the measurement campaign. The UAV is a six-wing model with height of 95 cm and width of 48 cm. The channel sounder on-board the UAV consists of a packaged discone antenna that receives the real-time downlink signals of live LTE networks, a USRP of type N210 [16], a small computer that controls the USRP and stores the received data and a GPS-disciplined oscillator that provides an accurate 10 MHz reference to the USRP. The radiation pattern of the discone antenna is nearly 3D omni-directional [5] to minimize its effect to the measured channels. In the measurement campaign, the downlink LTE signals were transmitted by the commercial BSs at the center frequency of 2.585 GHz with a bandwidth of 18 MHz. To effectively record the downlink LTE data, the USRP was tuned to receive the baseband data at the center frequency of 2.585 GHz with a complex sampling rate of 25 MHz. Readers may refer to [5] for details regarding the measurement equipment construction.

[1]For safety reasons, the lowest flight height was 35 meters in scenario B where there were many more buildings.

III. Interference investigation

A. Data processing

In the post-processing, channel impulse responses (CIRs) were extracted from the received downlink LTE data according to the LTE signal frame-structure as specified in [17]. The procedure mainly consists of three steps. Firstly, the data is filtered with bandwidth of 18 MHz to remove out-band signals and noise. Secondly, by exploiting the primary synchronization signal (PSS) and secondary synchronization signal (SSS), multiple cells are detected. Time synchronization for each cell is also obtained. Finally, CIRs for different channels between individual cells and the UAV are extracted by exploiting the cell specific reference signal (CRS) via inverse Discrete Fourier Transform (IDFT) [5], [18]–[22]. Specifically, let us denote the empirically received CRS as $r(\tau;t)$ and sent (or standard) CRS as $s(\tau;t)$ where t and τ indicate the observation time and excess delay, respectively. The CIR $h(\tau;t)$ is extracted as

$$h(\tau;t) = F^{-1}\{\frac{R(f;t)}{S(f;t)}\} \tag{1}$$

where F^{-1}, R and S denote the IDFT operation, frequency domain representation of r and frequency domain representation of s, respectively. Considering a multipath propagation channel, the empirically received CRS $r(\tau;t)$ from a cell reads

$$r(\tau;t) = r_c(\tau;t) + n(\tau) + n'(\tau) \tag{2}$$

with

$$r_c(\tau;t) = \sum_{\ell=1}^{L(t)} \alpha_\ell(t) s(\tau - \tau_\ell(t)) \tag{3}$$

where n denotes the complex Gaussian noise with power σ^2, α_ℓ and τ_ℓ represent the complex amplitude and delay of the ℓth propagation path, and L denotes the total path number. Note that n' in (2) denotes the interference from the other cells that transmit signals simultaneously. With multiple cells exist as interference sources, n' can also be considered as a complex Gaussian variable. According to (1)-(3), the spread function of $h(\tau;t)$ then reads

$$h(\tau;t) = \sum_{\ell=1}^{L(t)} \alpha_\ell(t)\sigma(\tau - \tau_\ell(t)) + n(\tau) + n'(\tau) \tag{4}$$

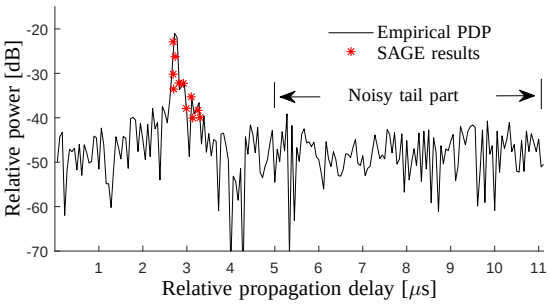

Fig. 3: An example PDP and SAGE estimation results.

Based on an instantaneous empirical CIR $h(\tau;t)$, a maximum-likelihood estimator is derived based on the SAGE principle to obtain estimates of the multipath parameters, namely $\hat{\alpha}_\ell$'s and $\hat{\tau}_\ell$'s, according to the signal model (4). Readers are referred to [23] for details of the SAGE algorithm. Fig. 3 illustrates an example instantaneous power delay profile (PDP) $|h(\tau;t)|^2$ and the corresponding SAGE estimation results. It is noteworthy that practically $L(t)$ is set adequately large to capture all the path parameters. The signal power $\hat{p}$ is calculated as the sum of all the $|\alpha_\ell|^2$ that are larger than the power of $(n'+n)$ which can be approximately as the variance of the tail part of the empirical CIR as illustrated in Fig. 3.

With $M(t)$ cells detected at time t, the estimated signal powers of the $M(t)$ cells are denoted as $\hat{p}_m, m = 1 \ldots M(t)$. To remove the small-scale fading effect, a window [24]–[26] with length of 20 wavelengths is applied to average the signal power $\hat{p}_m$. The signal-to-interference ratio (SIR) can then be calculated as

$$SIR = \frac{\hat{p}_{m_{\max}}}{\sum_{m \neq m_{\max}} \hat{p}_m} \tag{5}$$

where $\hat{p}_{m_{\max}}$ is the highest power among all $M(t)$ cells.[2] Moreover, a cell power can maintain the highest for some distance, and then power of another cell can exceed it (where handover could happen). We calculate the average distance where a cell always maintains the highest power as

$$d_a = \sum_i d_i \frac{d_i}{D} \tag{6}$$

where D is the whole horizontal distance, and d_i is the ith distance segment where a cell power is always the highest. d_a is essentially a weighted-average distance which provides insights on the handover rate of the aerial user equipment.

B. Scenario A

Fig. 4(a) illustrates the SIR variation along the horizontal distance at different heights for scenario A. Figs. 4(b)-(f) illustrate the power variations ($\hat{p}_m$) of all the detected cells at the five heights, respectively, where power variations of different cells are indicated with different colors in each figure. It can be observed from Fig. 4(a) that the SIR at the height of 15 m can exceed 15 dB. This is due to the high received power from the serving cell (i.e. $\hat{p}_{m_{\max}}$). Moreover, it can be observed from Fig. 4(b) that only 2 cells were detected at the height of 15 m. It is reasonable since the flight height is low and the ground environment can cause blockage to the neighboring cells, which also results in the low interference level. However, the SIR can also be low when the UAV is at the horizontal distance around 300 m. By observing Fig. 4(b), it can be inferred that the UAV was at the edge of two cells where the signal power of two cells are approximately the same, resulting in the low SIR. Generally, SIR decreases with the height increasing. It can be inferred from Figs. 4(b)-(f) that this is mainly due to two reasons. *i)* With height increasing, the received power of each cell decreases significantly. This is reasonable since the LTE networks are aimed for terrestrial coverage. *ii)* With higher heights, the ground objects are less likely to obstruct the link between a cell and the UAV, which can be testified by the fact that the maximal detectable cells number is 2, 3, 7, 7 and 11 respectively for the five heights from 15 m to 100 m. In

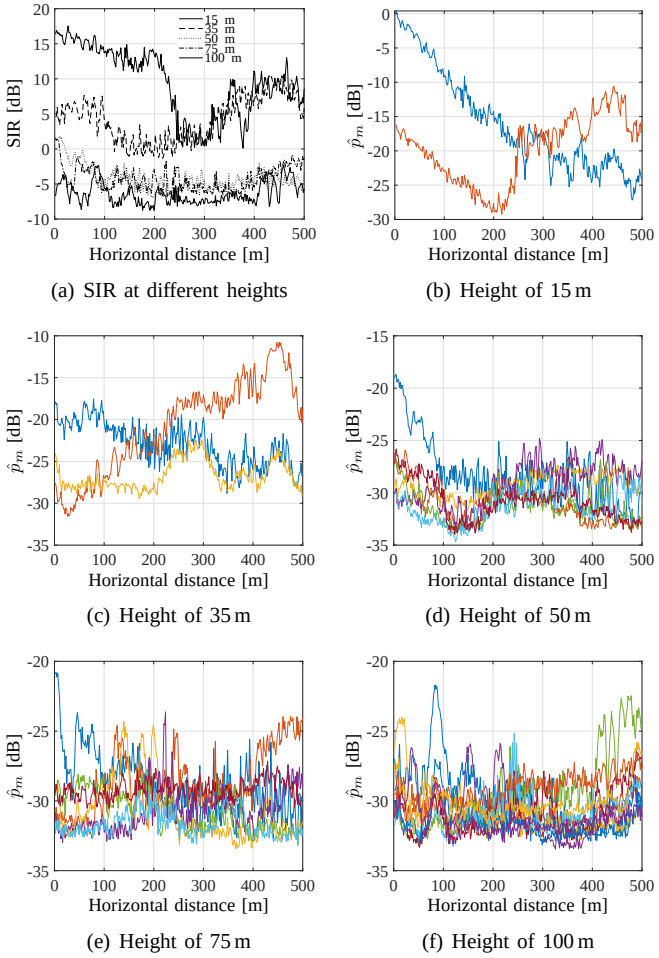

(a) SIR at different heights
(b) Height of 15 m
(c) Height of 35 m
(d) Height of 50 m
(e) Height of 75 m
(f) Height of 100 m

Fig. 4: SIR and power variations observed for different horizontal flights at scenario A.

[2]The SIR rather than signal-to-interference-plus-noise (SINR) is considered here for three reasons: *i)* SINR is a composite parameter that considers noise and interference together. It is not straightforward to find out the interference level from other cells. *ii)* Noise level may change, e.g. for different user devices due to their internal thermal noise. In which case, the SINR can not be applied for another device. *iii)* In a simulation, e.g. for performance evaluation, with signal power, noise level and SIR known, it is easy to retrieve SINR.

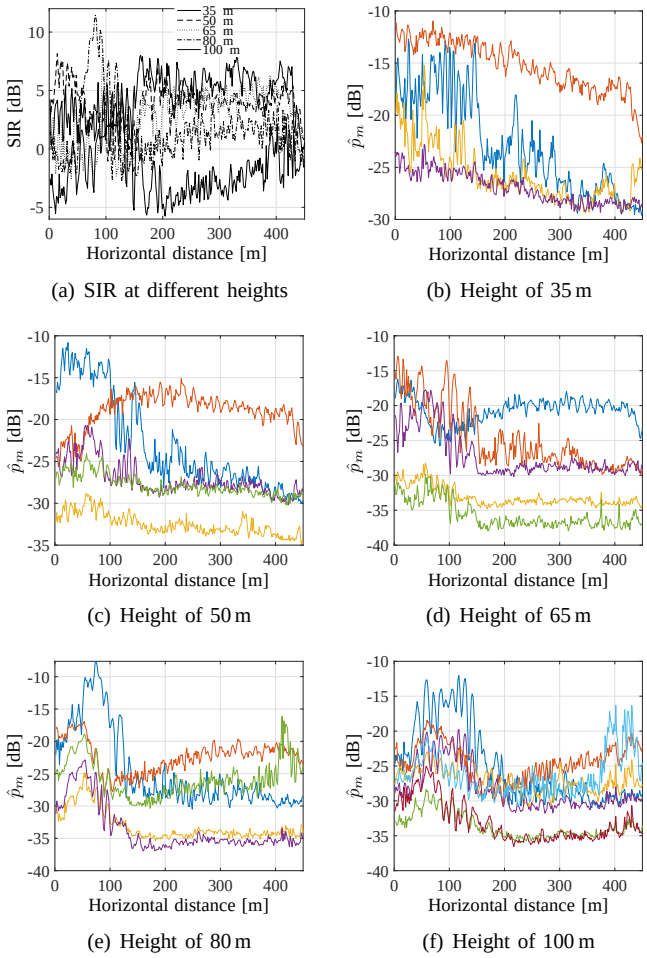

(a) SIR at different heights (b) Height of 35 m

(c) Height of 50 m (d) Height of 65 m

(e) Height of 80 m (f) Height of 100 m

Fig. 5: SIR and power variations observed for different horizontal flights at scenario B.

other words, the channel at higher height becomes more LoS-alike, and the interference from the other cells decreases the SIR significantly. For the same reason, handover could happen more frequently at higher heights. Calculations show that d_a decreases significantly with height increasing as 203, 191, 33, 33 and 20 m for the five flights, respectively.

C. Scenario B

Fig. 5(a) illustrates the SIR variation along the horizontal distance at different heights for scenario B, and Figs. 5(b)-(f) illustrate the power variations ($\hat{p}_m$) of all the detected cells at the five heights, respectively. Similarly, it can be observed from Fig. 5(a) that the SIR generally decreases with height increasing. The maximum detectable cells number was 4, 5, 5, 5 and 7 for the five heights, respectively. Compared to the cells number detected in scenario A, we have the following findings: *i)* The number of detected cells at lower heights in scenario B is larger than that of scenario A. For instance, the cells number at the height of 30 m was 3 and 4 for scenarios A and B, respectively. *ii)* However, for higher heights, the cells number detected in Scenario B is lower than that in Scenario A. For instance, the cells number at the height of 100 m was 11

Table I: Interference statistics for scenario A.

h [m]	SIR [dB], CDF at					d_i [m]		M
	0.15	0.4	0.65	0.9	1	Max	Mean (d_a)	
15	2.9	8.9	12.5	15.5	17.5	248	203	2
35	0.5	3.1	5.9	8.5	10.5	264	191	3
50	-5.9	-4.9	-3.9	-1.5	1.8	95	33	7
75	-6.0	-5.1	-3.7	-2.0	1.6	95	33	7
100	-7.8	-7.1	-6.3	-4.1	-2.3	51	20	11

Table II: Interference statistics for scenario B.

h [m]	SIR [dB], CDF at					d_i [m]		M
	0.15	0.4	0.65	0.9	1	Max	Mean (d_a)	
35	2.0	4.4	5.7	6.9	8.0	359	304	4
50	2.3	3.8	4.5	5.8	8.2	305	231	5
65	-0.4	2.8	4.2	5.4	8.1	299	204	5
80	-1.0	0.7	1.8	5.8	11.4	206	115	5
100	-4.1	-2.8	-1.3	1.6	4.4	90	34	7

and 7 for scenarios A and B, respectively. This is because in scenario A, the cells are mainly macro cells whose BS height and cell coverage are large, while scenario B is basically the dormitory area for students, and the cells are mainly micro cells with lower BS heights and smaller coverage. When the UAV is at lower heights, far neighboring cells are more likely to be blocked in scenario A. However, with height increasing more cells can be detected in scenario A due to the large coverage of each cell, which also results in lower SIR at higher heights compared to that in scenario B. In addition, calculations show that d_a in scenario B also decreases with height increasing, however, is larger than that in scenario A. They are calculated as 304, 231, 204, 115 and 34 m for the five horizontal flights, respectively. To summarize, Tables I and II include the extracted interference model parameters for scenarios A and B, respectively.

IV. Conclusions

In this letter, an interference investigation work for low-height air-to-ground channels was conducted based on field measurements in live LTE networks. Two different scenarios have been considered with horizontal flights at different heights. It is found that the SIR generally becomes lower at higher heights due to the clearance of the aerial channel links. This has been testified by the fact that more cells can be detected at higher heights, which also results in fast handover rate for both scenarios. Moreover, due to the large base-station heights and cell coverage, results show that in macro cells UAV can experience low interference level at lower heights where e.g. the SIR can be large as 17 dB at 15 m. Meanwhile, the SIR at higher heights e.g. 100 m can be severe as around -8 dB. As a contrast, due to smaller base-station heights and cell coverage in micro cells, the distinction of interference levels at different heights is not as obvious as that in macro cells. At lower heights, the SIR in micro cells is lower than that in macro cells, while at higher heights, the SIR in micro cells is larger than that in macro cells. In addition, faster handover rate can be observed in macro cells. The results obtained provide a valuable reference of interference levels for performance evaluation in live LTE networks for UAV communications.

REFERENCES

[1] Y. Zeng, R. Zhang, and T. J. Lim, "Wireless communications with unmanned aerial vehicles: opportunities and challenges," *IEEE Communications Magazine*, vol. 54, no. 5, pp. 36–42, May 2016.

[2] M. Bacco, A. Berton, A. Gotta, and L. Caviglione, "IEEE 802.15.4 air-ground UAV communications in smart farming scenarios," *IEEE Communications Letters*, vol. 22, no. 9, pp. 1910–1913, Sep. 2018.

[3] X. Chu, C. Briso, D. He, X. Yin, and J. Dou, "Channel modeling for low-altitude UAV in suburban environments based on ray tracer," in *12th European Conference on Antennas and Propagation (EuCAP 2018)*, April 2018, pp. 1–5.

[4] Z. Cui, C. Briso, K. Guan, D. W. Matolak, C. Calvo-Ramírez, B. Ai, and Z. Zhong, "Low-altitude UAV air-ground propagation channel measurement and analysis in a suburban environment at 3.9 GHz," *IET Microwaves, Antennas Propagation*, vol. 13, no. 9, pp. 1503–1508, 2019.

[5] X. Cai, J. Rodríguez-Piñeiro, X. Yin, N. Wang, B. Ai, G. F. Pedersen, and A. P. Yuste, "An empirical air-to-ground channel model based on passive measurements in LTE," *IEEE Transactions on Vehicular Technology*, vol. 68, no. 2, pp. 1140–1154, Feb 2019.

[6] E. R. S. Group *et al.*, "Roadmap for the integration of civil remotely-piloted aircraft systems into the European aviation system," *European RPAS Steering Group, Tech. Rep*, 2013.

[7] 3GPP, RP-170779, "New SID on enhanced support for aerial vehicles," NTT DOCOMO INC, Ericsson, 2017.

[8] 3GPP, RP-172669, "New WID on enhanced LTE support for aerial vehicles," NTT DOCOMO INC, Ericsson, 2017.

[9] R. He, W. Chen, B. Ai, A. F. Molisch, W. Wang, Z. Zhong, J. Yu, and S. Sangodoyin, "On the clustering of radio channel impulse responses using sparsity-based methods," *IEEE Transactions on Antennas and Propagation*, vol. 64, no. 6, pp. 2465–2474, June 2016.

[10] X. Cai, B. Peng, X. Yin, and A. P. Yuste, "Hough-transform-based cluster identification and modeling for V2V channels based on measurements," *IEEE Transactions on Vehicular Technology*, vol. 67, no. 5, pp. 3838–3852, May 2018.

[11] A. Al-Hourani and K. Gomez, "Modeling cellular-to-UAV path-loss for suburban environments," *IEEE Wireless Communications Letters*, vol. 7, no. 1, pp. 82–85, Feb 2018.

[12] R. Amorim, H. Nguyen, P. Mogensen, I. Z. Kovács, J. Wigard, and T. B. Sørensen, "Radio channel modeling for UAV communication over cellular networks," *IEEE Wireless Communications Letters*, vol. 6, no. 4, pp. 514–517, Aug 2017.

[13] B. Van Der Bergh, A. Chiumento, and S. Pollin, "LTE in the sky: trading off propagation benefits with interference costs for aerial nodes," *IEEE Communications Magazine*, vol. 54, no. 5, pp. 44–50, 2016.

[14] W. Mei and R. Zhang, "Uplink cooperative NOMA for cellular-connected UAV," *IEEE Journal of Selected Topics in Signal Processing*, vol. 13, no. 3, pp. 644–656, June 2019.

[15] T. Izydorczyk, M. Bucur, F. M. L. Tavares, G. Berardinelli, and P. Mogensen, "Experimental evaluation of multi-antenna receivers for UAV communication in live LTE networks," in *2018 IEEE Globecom Workshops (GC Wkshps)*, Dec 2018, pp. 1–6.

[16] "USRP N210 Datasheet," Tech. Rep. [Online]. Available: https://www.ettus.com/product/details/UN210-KIT

[17] "Evolved Universal Terrestrial Radio Access (E-UTRA); Physical channels and modulation," Tech. Rep., 3GPP TS 36.211 V14.3.0, Jun. 2017.

[18] X. Cai, A. Gonzalez-Plaza, D. Alonso, L. Zhang, C. B. Rodríguez, A. P. Yuste, and X. Yin, "Low altitude UAV propagation channel modelling," in *2017 11th European Conference on Antennas and Propagation (EUCAP)*, March 2017, pp. 1443–1447.

[19] X. Ye, X. Cai, Y. Shen, X. Yin, and X. Cheng, "A geometry-based path loss model for high-speed-train environments in LTE-A networks," in *International Conference on Computing, Networking and Communications (ICNC)*, Feb 2016, pp. 1–6.

[20] X. Ye, X. Yin, X. Cai, A. Pérez Yuste, and H. Xu, "Neural-network-assisted UE localization using radio-channel fingerprints in LTE networks," *IEEE Access*, vol. 5, pp. 12 071–12 087, 2017.

[21] X. Cai, N. Wang, J. Rodríguez-Piñeiro, X. Yin, A. P. Yuste, W. Fan, G. Zhang, G. F. Pedersen, and L. Tian, "Low altitude air-to-ground channel characterization in LTE network," in *13th European Conference on Antennas and Propagation (EuCAP)*, March 2019, pp. 1–5.

[22] X. Ye, X. Cai, X. Yin, J. Rodriguez-Pineiro, L. Tian, and J. Dou, "Air-to-ground big-data-assisted channel modeling based on passive sounding in LTE networks," in *IEEE Globecom Workshops (GC Wkshps)*, Dec 2017, pp. 1–6.

[23] B. H. Fleury, M. Tschudin, R. Heddergott, D. Dahlhaus, and K. Ingeman Pedersen, "Channel parameter estimation in mobile radio environments using the SAGE algorithm," *IEEE Journal on Selected Areas in Communications*, vol. 17, no. 3, pp. 434–450, March 1999.

[24] B. Zhang, Z. Zhong, R. He, F. Tufvesson, and B. Ai, "Measurement-based multiple-scattering model of small-scale fading in high-speed railway cutting scenarios," *IEEE Antennas and Wireless Propagation Letters*, vol. 16, pp. 1427–1430, 2017.

[25] R. He, Z. Zhong, B. Ai, and C. Oestges, "Shadow fading correlation in high-speed railway environments," *IEEE Transactions on Vehicular Technology*, vol. 64, no. 7, pp. 2762–2772, July 2015.

[26] W. C. Y. Lee, "Estimate of local average power of a mobile radio signal," *IEEE Transactions on Vehicular Technology*, vol. 34, no. 1, pp. 22–27, Feb 1985.